Frontiers of Environmental Science & Engineering
2025, 19(6): 76 https://doi.org/10.1007/s11783-025-1996-5

RESEARCH ARTICLE

Electrochemical treatment of bio-treated landfill leachate: Influence of electrode materials, current density, and sodium chloride concentration

Lina Wu[1], Yilan Yang[1], Yuhui Wang[1], Chenxu Wang[1], Yulin Zhang[1], Jiayuan Xu[1], Zhi Jiao[2], Yongzhen Peng ✉ [3]

1. Key Laboratory of Urban Stormwater System and Water Environment (Ministry of Education), Beijing University of Civil Engineering and Architecture, Beijing 100044, China
2. Shandong Borun Ecological Technology Company Limited, Heze 274000, China
3. National Engineering Laboratory for Advanced Municipal Wastewater Treatment and Reuse Technology, Engineering Research Centre of Beijing, Beijing University of Technology, Beijing 100124, China

HIGHLIGHTS

- Response surface methodology optimized parameters for maximal COD removal.
- Ti/PbO_2 presents better performance than Ti/SnO_2-Sb_2O_3 for pollutants removal.
- Both anodes completely removed NH_4^+-N, showing excellent nitrogen removal.
- TN removal capacity is in the following order: Pt < Ni < Steel cathodes.
- Ti/PbO_2 promotes the highest COD elimination rate was 99.91%.

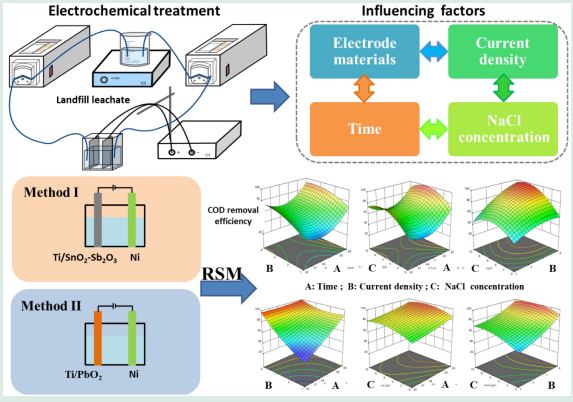

ABSTRACT: The landfill leachate harbors a substantial volume of pollutants necessitating their eradication prior to environmental release. In this investigation, the electrochemical oxidation of Biologically Treated Landfill Leachate (BTLL), following treatment via Upflow Anaerobic Sludge Blanket (UASB). This investigation delved into and compared with the impact of various operational parameters within the electrochemical oxidation process for both Ti/SnO_2-Sb_2O_3 and Ti/PbO_2 anodes—namely, current density, duration of operation, sodium chloride concentration, and cathode—on the efficiency of pollutant removal. Additionally, it employed response surface methodology to discern the optimal operational conditions for electrochemical oxidation of landfill leachate. The final experimental results indicate that under a current density of 50 mA/cm^2 and an electrolysis time of 4 h, the COD removal rates for Ti/SnO_2-Sb_2O_3 anode and Ti/PbO_2 anode were 79.48% and 92.31%, respectively, while the TN removal rates were 57.99% and 57.17%, respectively. Additionally, NH_4^+-N was completely removed for Ti/SnO_2-Sb_2O_3 anode and Ti/PbO_2 anode. Moreover, the former exhibited superior sewage treatment effectiveness when Ni was used as the cathode compared to Pt and steel. Response surface methodology (RSM) identified anode-specific optima: Ti/SnO_2-Sb_2O_3 (34 mA/cm^2,

✉ Corresponding author. E-mail: pyz@bjut.edu.cn
Article history: Received 2 January 2025, Revised 25 March 2025, Accepted 26 March 2025, Available online 15 April 2025

7.3 g/L NaCl) and Ti/PbO_2 (38 mA/cm^2, 6.0 g/L NaCl), both at 4 h, yielding COD removals of 93.6% and 97.2% (experimentally validated), respectively. This study provides novel theoretical support for the combined treatment of landfill leachate using biotreatment and chemical oxidation processes.

KEYWORDS: Ti/SnO_2-Sb_2O_3, Ti/PbO_2, Biologically treated landfill leachate, Electrochemical oxidation

1 Introduction

The escalating levels of urbanization and industrialization have precipitated a surge in the discharge of diverse forms of solid waste into the environment, anticipated to ascend to 3.6 billion tons by 2050 (Chen et al., 2020a; Li et al., 2023). Landfill leachate contains complex contaminants including refractory Chemical oxygen demand (COD), NH_4^+-N, and heavy metals (Miao et al., 2018; Zhao et al., 2021; Kan et al., 2023). While Upflow Anaerobic Sludge Blanket (UASB) reactors effectively remove organic matter and recover biogas during leachate pretreatment (Wu et al., 2019), their effluent often retains elevated COD levels requiring further treatment (Abdel-Shafy et al., 2022). Electrochemical oxidation (EO) has emerged as a promising solution due to its operational simplicity and high degradation efficiency for persistent pollutants (De Brito et al., 2019; Lindamulla et al., 2022; Fu et al., 2023). However, its high energy demand for complete mineralization necessitates energy-saving strategies. The integration of biological pre-treatment, specifically the UASB process, with electrochemical oxidation facilitated by Ti/SnO_2-Sb_2O_3 and Ti/PbO_2 anodes for landfill leachate treatment remains unexplored in the literature.

Electrochemical oxidation involves the passage of direct current through an electrolytic cell, initiating electrochemical, chemical, and physical reactions at the electrode-electrolyte interface (Särkkä et al., 2015; Iovino et al., 2023). The choice of anode material with optimal electrochemical properties is crucial for the efficiency of pollutant removal. Among the various anode materials studied, Ti/SnO_2-Sb_2O_3 electrodes and Ti/PbO_2 electrodes stand out for their performance in electrochemical oxidation processes. Ti/SnO_2-Sb_2O_3, while free from toxic metals, presents challenges such as complex fabrication, stringent doping requirements, and relatively lower stability compared to Ti/PbO_2 (Liu et al., 2023). On the other hand, Ti/PbO_2 electrodes exhibit high conductivity, strong oxidative properties, and efficient hydroxyl radical generation, which facilitate the complete mineralization of organic pollutants (Bao et al., 2023; Wang et al., 2024). Despite concerns regarding lead leaching from Ti/PbO_2 electrodes, prior studies indicate that the metal content in the electrolyte is minimal due to the anode's mechanical stability and the removal of metal ions via cathodic reduction during the degradation process (Ciríaco et al., 2009; Fernandes et al., 2014b).

The efficacy of EO treatment is influenced by electrode selection and operational parameters, with anode materials (Fernandes et al., 2014a) and pH effects (Luu, 2020; Wang et al., 2023) being well-characterized. However, the role of cathodes in pollutant removal and energy consumption remains underexplored. This study addresses this gap by comparing the performance of nickel foam, platinum, and steel cathodes, highlighting the impact of different anode-cathode configurations on pollutant treatment. Sodium chloride (NaCl) concentration is a key operational factor, directly affecting solution conductivity and the generation of active chlorine species, such as chlorine gas (Cl_2), hypochlorite ions (HOCl), and hydroxyl radicals (·OH), which are crucial for pollutant oxidation. Excessive NaCl concentrations can lead to chlorate and perchlorate by-products, making precise NaCl control essential to enhance treatment efficiency and minimize harmful by-products (Deng et al., 2019). In BTLL, typical NaCl concentrations range from 1500 to 12500 mg/L (Abdel-Shafy et al., 2022; Zheng et al., 2024), with values in this study ranging from 2500 to 2700 mg/L.

In this study, we deviate from the conventional single-factor experiments that have typically been employed to optimize electrochemical oxidation processes, and instead, we introduce Response Surface Methodology (RSM) to comprehensively analyze the interactive effects of current density, NaCl concentration, and reaction time. The present study employed a combination of UASB with Ti/SnO_2-Sb_2O_3 and Ti/PbO_2 electrodes for the electrochemical oxidation treatment of landfill leachate. We then investigated the impact of current density, operation time, sodium chloride concentration, and cathode type on the treatment efficiency of COD, TN, TOC, and ammonium nitrogen. Additionally, energy consumption was assessed. Utilizing RSM, we modeled and analyzed

the optimal operational conditions for electrochemical oxidation of landfill leachate with Ti/SnO_2-Sb_2O_3 and Ti/PbO_2 electrodes. This research presents a novel platform for the combined application of biological and chemical oxidation processes in the treatment of landfill leachate.

2 Materials and methods

2.1 Experimental preparation

The experiment utilized landfill leachate from the Shaanxi Weinan Majiagou Landfill, China (daily treatment capacity: 450 tons), which was pretreated by a UASB reactor (effective volume: 8.4 L; dimensions: D (diameter) × H (height) = 10 cm × 195 cm) and stored at low temperature. The leachate exhibited high organic load (COD: 1000–1200 mg/L) and ammonium nitrogen concentration (NH_4^+-N: 90–130 mg/L), with a conductivity of 19.56 mS/cm, making it suitable for electrochemical treatment (Table S1). Water quality parameters were analyzed using Chinese national standard methods: NH_4^+-N (HJ535-2009, Nessler's reagent method), COD (HJ/T399-2007, rapid digestion spectrophotometry), and total nitrogen (GB11894-1989, alkaline persulfate digestion UV method), measured via a Hach DR6000 analyzer (Germany). Three-dimensional excitation-emission matrix (3D-EEM) spectroscopy was performed on a Hitachi F-7000 fluorescence spectrophotometer (Hitachi High-Technologies Corporation, Japan) under the following conditions: emission wavelength 200–600 nm, excitation wavelength 200–500 nm, scan rate 12000 nm/min, and PMT voltage 500 V.

2.2 Electrochemical reactor

The experimental setup comprises an electrolytic cell, a peristaltic pump, a magnetic stirrer, and a power supply, as illustrated in Fig. S1. The electrolytic cell is constructed from acrylic material, with dimensions of 50 mm × 50 mm × 120 mm. The cathode comprises steel plate, nickel foam, and platinum plate (50 mm × 100 mm), whereas the anode is composed of a titanium plate coated with SnO_2-Sb_2O_3 and PbO_2 (50 mm × 100 mm, Ileka, China). The design of the electrochemical reactor incorporates a circulating electrolytic cell with an identical structure but varying anodes. An AC power supply (CT-4008-10V10A-A, Xinwei, China), featuring a voltage range of 220 V ± 10% and a frequency of 50/60Hz, was employed for the electrochemical reactions. A magnetic stirrer (Jintan Xinrui, China) was utilized to ensure the uniform distribution of the electrolyte within the system. According to the experimental design, the anode and cathode are placed parallel to each other, with a constant gap (2 cm) maintained between them. 400 mL of garbage leachate treated by UASB is transferred to a beaker, and then a peristaltic pump (Longer Pump, China) is employed to circulate the electrolyte at a flow rate of 60 mL/min under different experimental conditions, consistent with previous studies (Abbasi et al., 2020; Zhou et al., 2020).

2.3 Experimental operation mode

The factors influencing the efficiency of COD, TN, TOC, and ammonia nitrogen removal in the EO process were investigated. These factors include the type of anode material (Ti/SnO_2-Sb_2O_3 electrode and Ti/PbO_2 electrode), cathode material (Ni, Pt, and steel), sodium chloride concentration (0, 3, and 10 g/L), and current density (30, 50, and 65 mA/cm^2). Specific experimental conditions are detailed in Table S2. Samples were withdrawn from the reactor at reaction times of 0, 30, 60, 90, 120, 150, 180, and 240 min for subsequent analysis. Samples were collected during the reaction process using a sterilized syringe and subsequently filtered through a 0.45 μm membrane for the determination of various parameters.

2.4 Basic principle of electrochemical oxidation

Mechanism of COD removal by electrochemical oxidation (EO) operates through two distinct pathways (Panizza and Martinez-Huitle, 2013): 1) Direct Oxidation: organic pollutants (R) adsorb onto anode active sites (M), undergoing electron transfer, as shown in Eq. (1). Limited by anode passivation at high pollutant concentrations (He et al., 2019). 2) Indirect oxidation: Generates reactive species through hydroxyl radicals and chlorine species, as shown in Eqs. (2) and (3) (Lee et al., 2022). These mediators degrade 60%–80% organics in chloride-rich landfill leachate (Zhu et al., 2008; Sun et al., 2021).

$$M + R \rightarrow M(\cdot R) + e^- \quad (1)$$

$$M + H_2O \rightarrow M(\cdot OH) + H^+ + e^- \quad (2)$$

$$M(\cdot OH) + R \rightarrow M + RO + H^+ + e^- \quad (3)$$

Mechanism of NH_4^+-N removal by electrochemical oxidation primarily occurs through direct oxidation (anodic electron transfer converting NH_3 to N_2) and

indirect oxidation mediated by active chlorine species (generated via chloride electrolysis), as shown in Eqs. (4)–(9), when the concentration of chloride ions in wastewater exceeds 300 mg/L, indirect oxidation proves more cost-effective and efficient than direct oxidation (Qiang and Adams, 2004). However, due to active chlorine's simultaneous involvement in the indirect oxidation of COD and ammonia nitrogen, a competitive relationship exists between the removal efficiencies of these two pollutants (Deng and Englehardt, 2007). Chen (2008) found that EO can simultaneously remove COD and NH_4^+-N, during oxidation, NH_4^+-N removal occurs first, followed by an increase in COD degradation after its completion.

$$2NH_3 + 6OH^- \rightarrow N_2 + 6H_2O + 6e^- \quad (4)$$

$$M + 2Cl^- \rightarrow M + Cl_2 + 2e^- \quad (5)$$

$$Cl_2 + H_2O \rightarrow HClO + H^+ + Cl^- \quad (6)$$

$$NH_4^+ + HClO \rightarrow NH_2Cl + H^+ + H_2O \quad (7)$$

$$NH_2Cl + HClO \rightarrow NOH + 2H^+ + 2Cl \quad (8)$$

$$NH_2Cl + NOH \rightarrow N_2 \uparrow + H^+ + Cl^- + H_2O \quad (9)$$

3 Results and discussion

3.1 Effect of anode and current density

3.1.1 COD and TOC removal rate

In Fig. 1, the bar chart denotes the quantity of the target analyte (right *y*-axis,) while the line chart denotes the percentage removal of the analyte (left *y*-axis). Figure 1(1) illustrates COD and TOC removal efficiencies of Ti/SnO_2-Sb_2O_3 and Ti/PbO_2 anodes across varying current densities. The Ti/PbO_2 anode consistently achieved higher COD removal rates than Ti/SnO_2-Sb_2O_3 across all tested conditions. For instance, at 50 mA/cm^2 after 4 h, Ti/PbO_2 removed 92.31% COD (effluent: 89 mg/L), meeting the national comprehensive sewage discharge standard GB 8978-1996, while Ti/SnO_2-Sb_2O_3 attained 79.48%. This disparity stems from divergent oxidation mechanisms: Ti/PbO_2 leverages indirect oxidation via ClO^-/ClO_2^- species generated electrochemically from NaCl, favored by its lower oxygen evolution potential (OEP, 1.75 V), which minimizes energy dissipation toward parasitic oxygen evolution (Comninellis, 1994; Zhao et al., 2010). Conversely, Ti/SnO_2-Sb_2O_3 relies predominantly on direct hydroxyl radicals (·OH)-mediated oxidation due to its higher OEP (1.98 V), but suffers from ·OH scavenging by chloride ions and slower charge transfer kinetics (Chen et al., 2020b). At 65 mA/cm^2, near-identical TOC removal for both anodes suggests comparable mineralization capacity via ·OH generation (Luu, 2020), consistent with Cossu et al. (1998). Notably, Ti/PbO_2's superior COD efficiency at high current densities (e.g., 97.47% at 65 mA/cm^2 vs. 92.31% at 50 mA/cm^2) highlights its robustness in degrading recalcitrant organics. The trend in COD removal aligns with the findings of Fernandes et al. (2016).

3.1.2 Ammonia nitrogen and TN removal rate

Figure 1(2) depicts the removal efficiencies of ammonia nitrogen (NH_4^+-N) and total nitrogen by Ti/PbO_2 and Ti/SnO_2-Sb_2O_3 anodes in leachate. Both achieved complete NH_4^+-N removal (> 99%) across 30 to 65 mA/cm^2 after 4 h, outperforming prior studies (e.g., 40% at 70 mA/cm^2 in Fernandes et al. (2016), due to optimized indirect oxidation via active chlorine (ClO^-/ClO_2^-) generated from NaCl. However, Ti/SnO_2-Sb_2O_3 exhibited marginally higher TN removal (68% vs. 60% for Ti/PbO_2 at 65 mA/cm^2, attributed to its dual mechanism: 1) Cathodic Nitrate Reduction: Enhanced NO_3^--N reduction to N_2 at Ni cathodes (used with Ti/SnO_2-Sb_2O_3), favored by its high hydrogen evolution overpotential, maximizing electron allocation to nitrate reduction over H_2 generation (Shih and Hsu, 2021). 2) Anodic Oxidation Pathways: Ti/PbO_2's lower OEP (1.75 V) prioritizes indirect oxidation, generating excess ClO^- that non-selectively oxidizes both organics and NH_4^+-N, limiting electrons for cathodic NO_3^- reduction (Zhao et al., 2010). In contrast, Ti/SnO_2-Sb_2O_3's higher OEP (1.98 V) sustains ·OH-driven NH_4^+-N oxidation while preserving cathode efficiency for NO_3^- to N_2 conversion (Chen et al., 2020b).

3.2 Effect of cathode

3.2.1 Ti/SnO_2-Sb_2O_3 as anode

Figure 1(3) demonstrates the removal efficiencies of COD, TOC, NH_4^+-N, and TN from BTLL by electrolysis of Ti/SnO_2-Sb_2O_3 as anode with different cathode (Ni, Pt and steel) combinations at a current density of 50 mA/cm^2 for 240 min. The results reveal that when Ni serves as the cathode, it yields the most favorable COD removal efficiency at 79%, whereas the disparity in COD removal efficiency between Pt and steel cathodes is marginal, at 68% and 69%,

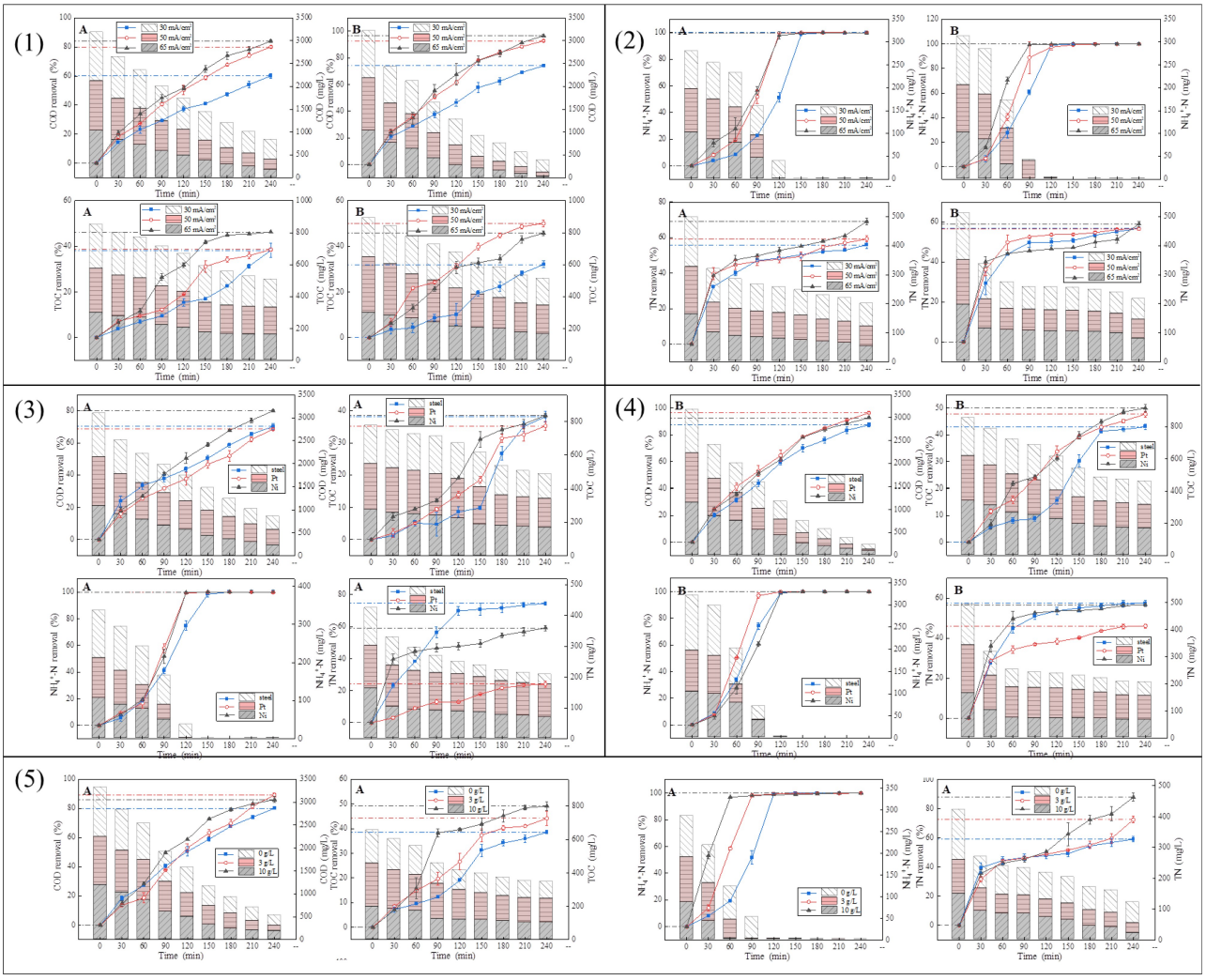

Fig. 1 COD, TN, TOC, and NH_4^+-N elimination rate (%) at different current densities, different cathodes and different concentrations of NaCl of (A) Ti/SnO_2-Sb_2O_3 and (B) Ti/PbO_2 anodes.

respectively. During the reaction, the dissolution of steel from the cathode surface into the solution may lead to the formation of amorphous substances to a certain extent, causing electrode corrosion, thereby impeding the progress of the reaction (Van Ede et al., 2024). There is no significant difference in the removal efficiency of TOC among the three, indicating comparable levels of mineralization. At 120 min of electrolysis, Pt and Ni have achieved 100% removal efficiency for NH_4^+-N, while steel reaches 100% removal after 150 min of electrolysis. Their ability to remove TN follows the sequence: Pt < Ni < steel. Different cathodes primarily affect the removal of TN, with minimal impact on the removal of COD, TOC, and NH_4^+-N. Overall, when combined with Ni, Ti/SnO_2-Sb_2O_3 exhibits superior performance in wastewater treatment compared to its combination with Pt and steel.

3.2.2 Ti/PbO_2 as anode

Under the condition of an electrolysis current density of 50 mA/cm^2, Ti/PbO_2 as the anode is combined with different cathodes (Ni, Pt, and steel) to evaluate their removal efficiency for COD, TOC, NH_4^+-N, and TN. Results in Fig. 1(4) demonstrate that after 240 min of electrolysis, the removal efficiency of COD follows the sequence: Pt > Ni > steel, with removal rates of 97%, 92%, and 88%, respectively. At 90 min of electrolysis, Pt has achieved 100% removal efficiency for NH_4^+-N, while Ni and steel reach 100% removal at 120 min of electrolysis for NH_4^+-N. Moreover, it is observed that after 60 min of electrolysis, the curve of TN removal rate tends to flatten, possibly due to the rapid generation

of chlorine gas at high current densities over extended periods, leading to partial overflow of the solution. Overall, Ti/PbO_2 exhibits the best performance in TOC removal when combined with Ni, achieves the highest COD removal when combined with Pt, and demonstrates the best TN removal when combined with steel. Rao et al. (2019) conducted an EO reaction using a Ti/PbO_2 anode at a current density of 40 mA/cm^2 and an electrolysis duration of 120 min, comparing the influence of different cathodes on nitrate removal, including carbon paper (C) and titanium (Ti), iron (Fe), copper (Cu), and aluminum (Al) plates. The study reveals a sequential decrease in cathodic nitrate removal efficiency as follows: C > Ti = Fe > Cu > Al.

3.3 Effect of initial NaCl concentration

The Ti/PbO_2 anode exhibits superior pollutant removal efficiency over Ti/SnO_2-Sb_2O_3. To elucidate the role of chloride-mediated indirect oxidation, we evaluated NaCl concentration effects (0–10 g/L) on Ti/SnO_2-Sb_2O_3 performance at 50 mA/cm^2 (Ni cathode, 4 h). COD removal peaked at 88% with 3 g/L NaCl but declined to 85% at 10 g/L, whereas TOC, NH_4^+-N, and TN removal consistently improved with increasing NaCl (Fig. 1(5)). This divergence highlights that active chlorine species (ClO^-/ClO_2^-) preferentially drive NH_4^+-N and TN oxidation via indirect pathways, while COD removal involves competitive consumption of ClO^- between organics and ammonia (Mandal et al., 2020). Notably, Mandal's study corroborates Cl^-'s critical role in enhancing COD, dissolved organic carbon (DOC), and NH_4^+-N removal, contrasting with inhibitory effects of SO_4^{2-}, NO_3^-, and HCO_3^-. These findings underscore NaCl concentration as a pivotal factor in balancing direct (·OH) and indirect (ClO^-) oxidation pathways, optimizing electrochemical treatment efficacy for multi-pollutant systems.

3.4 Treatment efficiency analysis

3.4.1 Three-dimensional fluorescence spectrum analysis

The dissolved organic matter in the fluorescence spectrum can be classified into five major categories: aromatic proteins, aromatic proteins II, fulvic acids, microbial byproducts, and humic acids (He et al., 2011). Figure 2 illustrates the results of the Excitation-Emission Matrix (EEM) of organic matter in sewage treated by UASB, revealing the presence of fluorescence peaks of humic acid and fulvic acid, with intensities of 6988 and 1408 au, respectively. Their wavelength ranges are Ex/Em = (250–400) nm/(380–500) nm and Ex/Em = (220–250) nm/(380–500) nm (Komatsu et al., 2025), indicating that humic acid and fulvic acid are the main pollutants in biologically treated sewage. Additionally, there are characteristic peaks of microbial byproducts, with a wavelength range of Ex/Em = (250–280) nm/(280–380) nm.

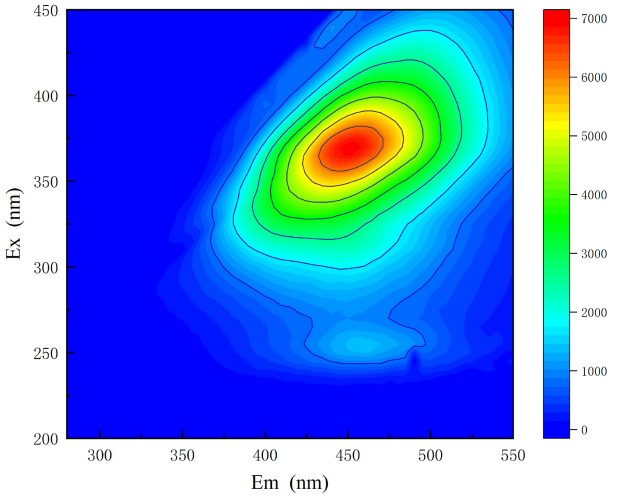

Fig. 2 EEM of biologically treated wastewater.

Figure 3 demonstrates humic acid (HA) and fulvic acid (FA) degradation dynamics during electrochemical oxidation (EO) under varied current densities and NaCl concentrations. At 3 g/L NaCl, 50 mA/cm^2 achieved optimal removal efficiencies for both HA (97.40%, 182 au) and FA (95.38%, 65 au) after 240 min, surpassing 30 mA/cm^2 (HA: 97.07%, 205 au; FA: 92.90%, 100 au) and 65 mA/cm^2 (HA: 96.63%, 235 au; FA: 92.19%, 110 au). FA degradation (complete by 120 min) consistently preceded HA elimination (complete by 180 min), reflecting preferential oxidation of soluble low-molecular-weight FA over complex HA. Increasing NaCl to 10 g/L (65 mA/cm^2) accelerated HA degradation, reducing fluorescence intensity to 205 au (97.07% removal) at 120 min and 98 au at 240 min. Fluorescence shifts revealed preferential degradation of simpler organics (shorter-wavelength peaks, e.g., protein-like substances at 280 nm), while humic substances are initially degraded into small molecular humic substances, subsequently transforming into macromolecular substances resembling proteins (e.g., lipids, proteins, and carbohydrates) and soluble microbial degradation products (SMDP), which are less readily utilized by microorganisms (He et al., 2013). These results highlight the dual role of current density (maximizing oxidation efficiency at 50 mA/cm^2) and NaCl (accelerating kinetics via active chlorine pathways), offering actionable insights for tailoring EO to target specific organic fractions in landfill leachate.

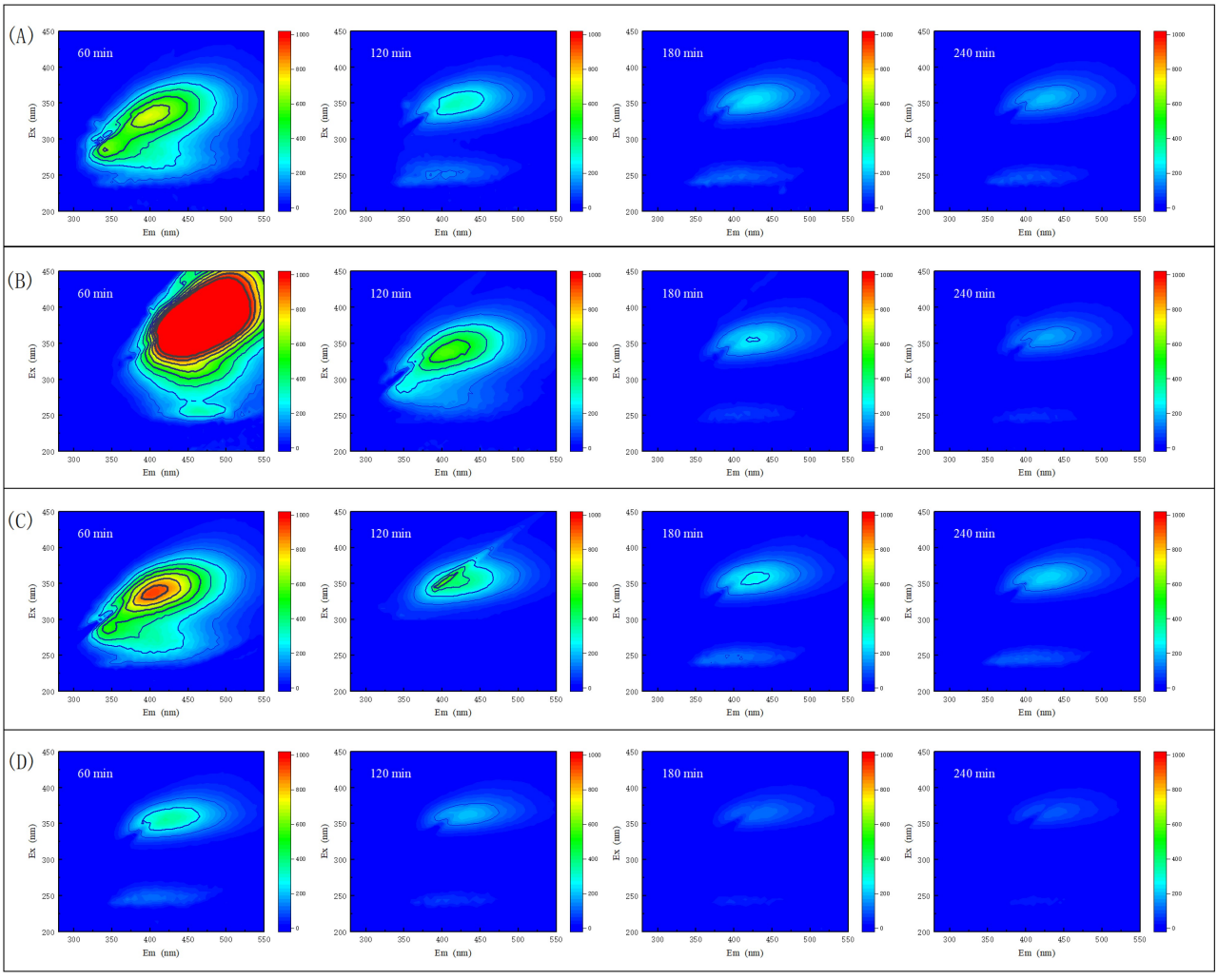

Fig. 3 The EEM of dissolved organic matter during electrolysis, with reaction conditions as follows: (A) NaCl concentration of 3 g/L and current density of 30 mA/cm^2; (B) NaCl concentration of 3 g/L and current density of 50 mA/cm^2; (C) NaCl of 3 g/L and current density of 65 mA/cm^2; (D) NaCl of 10 g/L and current density of 65 mA/cm^2.

3.4.2 Ultraviolet and Fourier Transform Infrared spectrum analysis

Figure 4(A) illustrates the Ultraviolet (UV) absorption spectra corresponding to varying treatment durations during the reaction. UV absorption spectra, resulting from electronic transitions, elucidate the conjugation relationships inherent to unsaturated groups. Larger molecules, characterized by elevated levels of aromatic and conjugated double bond structures relative to smaller molecules, demonstrate significantly greater UV absorption intensities per mole (He et al., 2012). Furthermore, a multitude of pronounced absorption peaks is observed in the UV region spanning from 200 to 220 nm, indicating the presence of diverse macromolecular organic compounds characterized by conjugated double bonds and carbonyl groups, along with polycyclic aromatic compounds in the leachate. During the initial 0 to 60 min following the initiation of the reaction, a rapid decline in absorbance is observed. This observation implies that substantial macromolecular organic compounds are undergoing oxidation processes that yield carbon dioxide, water, and smaller organic molecules. The absorbance ratio at 250 to 365 nm (E_{250}/E_{365}) in ultraviolet spectra demonstrates a negative correlation with the degree of humification, aromatic polymerization, and relative molecular weight (Xi et al., 2012). $SUVA_{254}$ serves as a widely accepted indicator for characterizing the aromaticity of organic substances (Sharma et al., 2024). This parameter exhibits a positive correlation with the concentration of aromatic compounds. Following a reaction duration of 240 min, E_{250}/E_{365} increased from

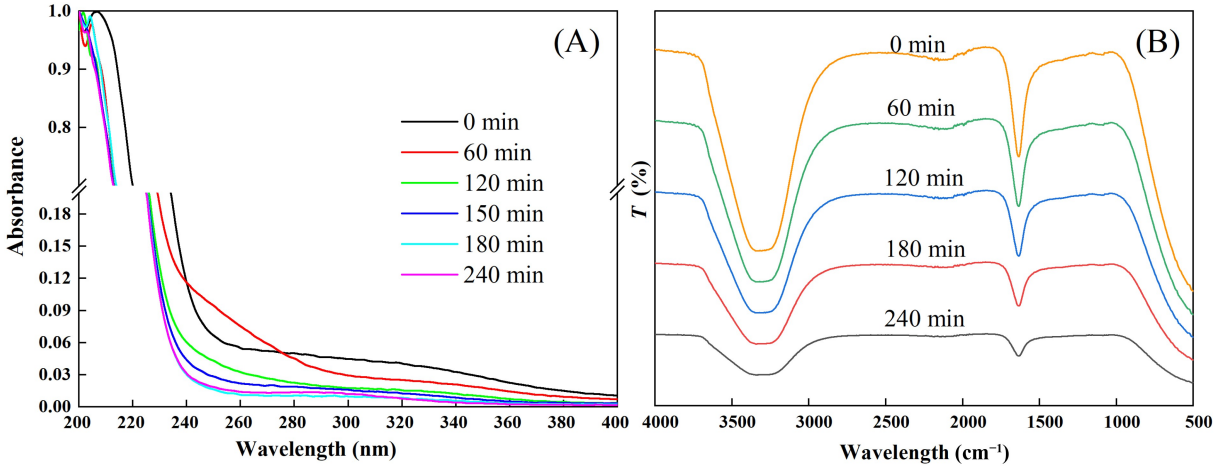

Fig. 4 The UV spectrum and FTIR spectrum during electrolysis. (A) UV spectrum; (B) FTIR spectrum. (Current density: 50 mA/cm^2, electrode anodes: Ti/SnO_2-Sb_2O_3).

3.124 to 9.910, whereas $SUVA_{254}$ diminished from 0.169 to 0.056, thereby indicating that the electrolysis process effectively reduces the aromaticity and molecular weight of organic substances present in landfill leachate.

The Fourier Transform Infrared (FTIR) spectra of landfill leachate subjected to electrolysis for varying durations are illustrated in Fig. 4(B). Within the spectral range of 1900 to 2500 cm^{-1}, numerous minor peaks are observed, which are attributed to the stretching vibrations of C ≡ C or C ≡ N, in addition to asymmetric stretching vibrations of cumulative double bonds such as C = C = C and C = C = O. The characteristic peaks of aromatic C = C bonds (1690 to 1580 cm^{-1}) and adjacent absorption peaks corresponding to amide substances (primarily resulting from protein degradation) as well as phenolic hydroxyl and carboxylic compounds exhibit diminishing peak intensity and narrowing peak shape as the treatment duration increases, thereby indicating the removal of certain amide substances along with phenolic hydroxyl and carboxylic compounds (Rigotto et al., 2023).

3.5 Energy consumption

The energy consumption is calculated by Eq. (10) (Tien and Luu, 2020), where t represents the reaction time in hours, C denotes the average voltage during operation (V), I signifies the average applied current (A), COD stands for the concentration of chemical oxygen demand (COD) after time t (mg/L), and Sv represents the volume of filtrate (L).

$$EC = \frac{t \times I \times C \times 10^3}{\Delta \mathrm{COD} \times Sv}. \quad (10)$$

Figure 5 illustrates the energy consumption of two anodes (Ti/SnO_2-Sb_2O_3 and Ti/PbO_2) paired with different cathodes (Ni, Pt, and steel) under a current density of 50 mA/cm^2. The energy consumption ranges for Ti/SnO_2-Sb_2O_3 anode are from 58 to 141 kWh/kg COD, and for Ti/PbO_2 anode, the range is from 51 to 94 kWh/kg COD. Within the electrolysis period of 1 to 4 h, the energy consumption of Ti/SnO_2-Sb_2O_3 anode is significantly higher than that of Ti/PbO_2 anode. The cathodic energy consumption increases in the following order: Ni < Pt < steel.

3.6 Response surface methodology for process optimisation

To identify optimal operating conditions for electrochemical oxidation using two anodes (Ti/SnO_2-Sb_2O_3 and Ti/PbO_2) paired with a nickel foam cathode, this study employed response surface methodology (RSM). Three variables—current density (A), electrolysis time (B), and sodium chloride concentration (C)—were selected as independent parameters, with COD removal efficiency as the response variable. RSM, a statistical optimization technique, establishes relationships between input factors and output responses through multivariate quadratic models, enabling systematic exploration of process variables.

The methodology of response surface analysis constitutes a statistical approach to experimental design that allows for rational experimental structuring and the modeling of functional dependencies between factors and response variables through a multivariate quadratic regression equation. The experimental design in this investigation utilized the Box-Behnken central

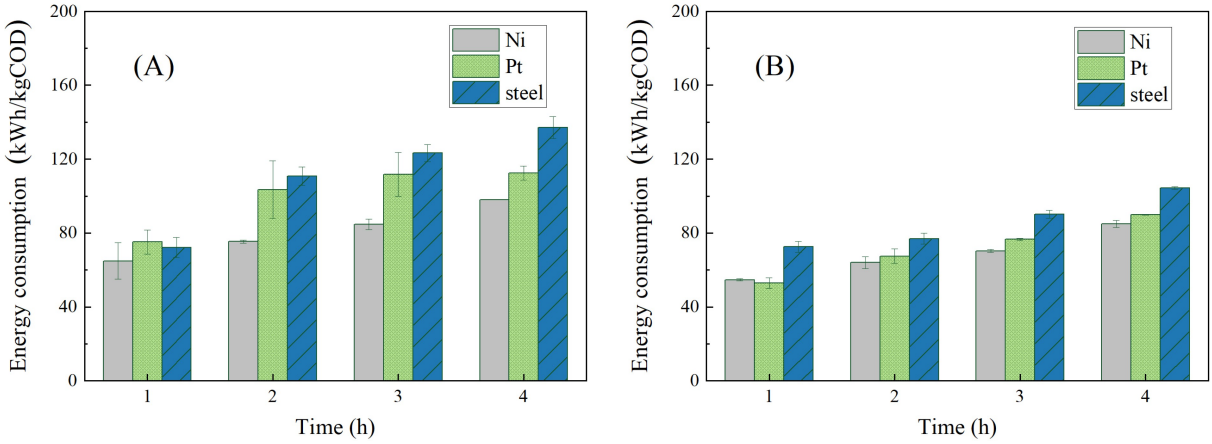

Fig. 5 Energy consumption of (A) Ti/SnO_2-Sb_2O_3; (B) Ti/PbO_2 anodes at 50 mA/cm^2.

composite methodology, wherein the coding scheme for the influencing factors and their respective levels is delineated in Table S3. The selection of influencing factors and their corresponding value ranges were determined via single-factor experiments. The experimental results obtained with Ti/SnO_2-Sb_2O_3 as the anode are presented in Table S4, while the experimental results obtained with Ti/PbO_2 as the anode are listed in Table S5.

From the outcomes displayed in Table S4, it is evident that the experimental model's F-value stands at 36.49 with $P < 0.001$ when employing Ti/SnO_2-Sb_2O_3 anodic electrolysis, denoting a notable correlation between COD removal rate and said model. Simultaneously, the insignificance of the model's misfit ($P = 0.2313$, $R_{adj}^2 = 0.9523$) suggests the suitability of this quadratic polynomial model as a predictor for COD removal rate, elucidating 95.23% of the variance in response values, and boasting an adequate precision exceeding 4, indicative of substantial information explicable by the model. A P-value of ⩽ 0.05 signifies a significant impact of the factor on COD removal rate. Variance analysis delineates that current density (A), reaction time (B), and sodium chloride concentration (C)—coefficients in Eq. (11)—all exert significant influences on COD removal rate, ordered by impact strength as reaction time > sodium chloride concentration > current density. Furthermore, the P-value for the interaction term BC falls below 0.05, signifying a conspicuous interaction between reaction time and sodium chloride concentration concerning electrolysis time, significantly impacting COD removal rate. Post elimination of non-significant factors, the response surface method yields the fitted equation for COD removal rate during Ti/SnO_2-Sb_2O_3 anodic electrolysis as represented in Eq. (11).

$$Y = 71.54 + 9.01A + 17.82B + 11.9C - 1.73AB - 1.67AC + 8.85BC + 21.23A^2 - 7.94B^2 - 18.11C^2. \quad (11)$$

To analyze the interactive effects of current density, reaction time, and sodium chloride concentration on COD removal efficiency during Ti/SnO_2-Sb_2O_3 anode electrolysis, response surface analysis will be conducted using the aforementioned data. Figure 6(A) illustrates the effects of current intensity and reaction time on COD removal efficiency under constant sodium chloride concentration. COD removal efficiency exhibited a nonlinear relationship with current density at fixed reaction times. Initially, efficiency decreased (e.g., 30–50 mA/cm^2) due to competing oxygen evolution reactions (OER) consuming hydroxyl radicals (·OH), but rebounded at higher densities (50–65 mA/cm^2) as enhanced ·OH generation offset OER losses (Duan et al., 2020). Prolonging reaction time significantly improved efficiency under high current densities (> 50 mA/cm^2), evidenced by denser contour lines in this regime (Fig. 6(A)), whereas low-current conditions (< 50 mA/cm^2) showed minimal time dependency. Depicted in Fig. 6(B), at high current densities (> 50 mA/cm^2), COD removal efficiency increased with NaCl concentration (3–10 g/L), driven by active chlorine (ClO^-/ClO_2^-) production. Conversely, under low current densities (< 50 mA/cm^2), elevated NaCl (> 5 g/L) reduced efficiency due to insufficient Cl^- activation, leading to salt-layer accumulation and impaired ·OH availability. Figure 6(C) presents the response surface analysis (RSM) of COD removal efficiency as a function of reaction time and NaCl concentration under fixed current density. The nonlinear interaction reveals that at shorter durations (< 2 h), increasing NaCl initially enhances COD removal (via ClO^- generation) but subsequently reduces efficiency at higher NaCl concentrations (>

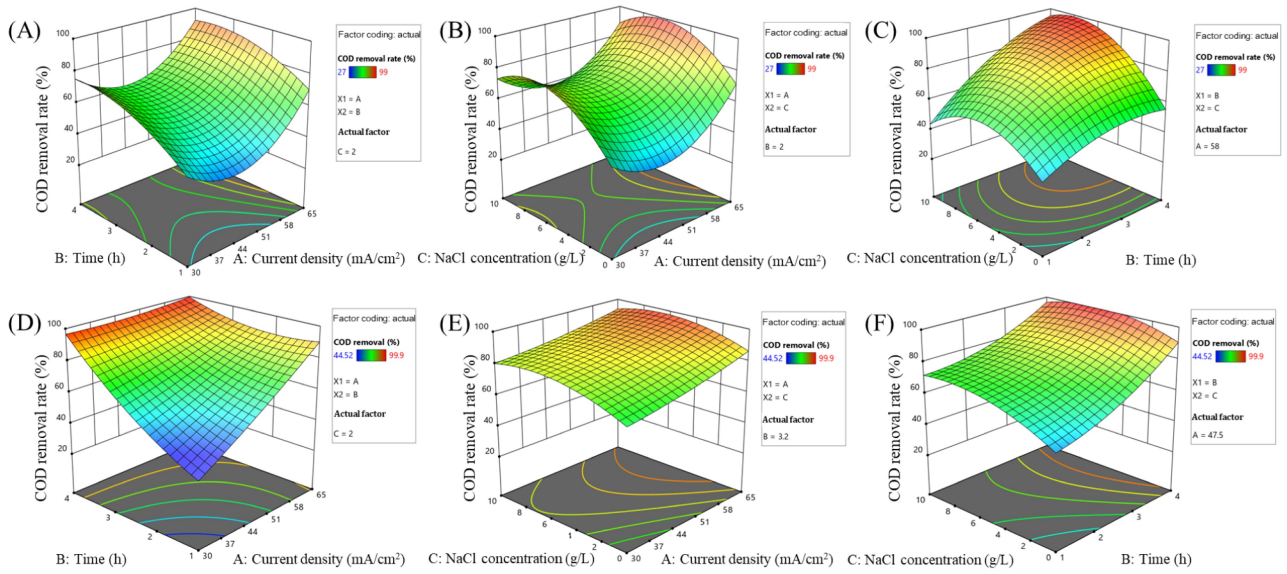

Fig. 6 Response surface of COD removal when the anode of (A–C) Ti/SnO_2-Sb_2O_3 and (D–F) Ti/PbO_2 anodes.

5 g/L), likely due to incomplete Cl^- activation and salt-layer formation on the anode surface, which impedes mass transfer and ·OH generation (Sun, 2008). RSM-predicted optimal conditions (34 mA/cm^2, 7.3 g/L NaCl, 4 h) yielded a COD removal efficiency of 94.2%.

To validate these predictions experimentally, we conducted triplicate runs under the RSM-optimized parameters for the Ti/SnO_2-Sb_2O_3 anode, achieving a COD removal of 93.6% ± 0.8% (Fig. S2), confirming the model's accuracy (< 2% deviation). Further, comparative tests at suboptimal conditions (e.g., 50 mA/cm^2, 3 g/L NaCl, 4 h) resulted in lower COD removal (79.5% vs. 93.6%), corroborating the necessity of balancing NaCl concentration and reaction time to maximize ClO^- utilization.

From the results presented in Table S5, it is evident that when employing Ti/PbO_2 anode electrolysis, the experimental model yields an F value of 78.48 with $P <$ 0.001, indicating a significant relationship between COD removal efficiency and the model. Moreover, the lack of fit of the model is not significant (P = 0.2476, R_{adj}^2 = 0.9735), indicating that this quadratic polynomial model is suitable as a predictive model for COD removal efficiency, capable of explaining 97.35% of the variation in response, with an adequate precision greater than 4, demonstrating excellent fitting precision of the regression equation. The analysis of variance results indicate that current density (A), reaction time (B), and sodium chloride concentration (C)—coefficients in Eq. (12)—significantly affect the COD removal rate, with the influence ranking in the order of reaction time > current density > sodium chloride concentration. Furthermore, the interaction term AB exhibits a P-value of less than 0.05, indicating a significant interaction between current density and electrolysis time, with this interaction significantly impacting the COD removal rate. After excluding non-significant factors, the response surface methodology yields the fitted equation for COD removal rate during Ti/PbO_2 anodic oxidation, as illustrated by Eq. (12).

$$Y = 85.34 + 9.39A + 13.01B + 5.09C - 8.60AB - 1.13AC - 2.15BC + 1.54A^2 + 2.61B^2 - 7.36C^2. \quad (12)$$

To analyze the interactive effects of current density, reaction time, and sodium chloride concentration on the COD removal rate during Ti/PbO_2 anodic electrolysis, response surface analysis will be conducted based on the data presented above. Response surface analysis (Figs. 6(D)–6(F)) elucidates the interplay of current density (30–65 mA/cm^2), reaction time (1–4 h), and NaCl concentration (0–10 g/L) on COD removal during Ti/PbO_2 anodic electrolysis. At low current densities (< 38 mA/cm^2), COD removal efficiency increased with reaction time extension (Fig. 6(D)), aligning with electron transfer-controlled oxidation kinetics (Kapałka et al., 2010). Conversely, at higher current densities (> 50 mA/cm^2), mass transfer limitations dominated, reducing time dependency. Figure 6(E) reveals NaCl's dual role: under high current density, COD removal improved with NaCl concentration (3–10 g/L) via enhanced ClO^- generation, whereas low current densities (< 38 mA/cm^2) exhibited a peak due to incomplete Cl^- activation and salt-layer passivation. Figure 6(F) further highlights reaction time's criticality at low NaCl concentrations (< 3 g/L), where prolonged electrolysis (> 3 h) compensated for limited ClO^-

availability. Multi-response optimization identified 38 mA/cm^2, 6.0 g/L NaCl, and 4 h as optimal parameters (predicted COD removal: 99.9%).

To confirm the practical relevance of these statistically derived conditions, triplicate experiments were conducted under RSM-optimized settings (38 mA/cm^2, 6.0 g/L NaCl, 4 h). The results demonstrated a COD removal efficiency of 98.9% ± 0.6% (Fig. S2), closely aligning with the model's prediction (99.9%). Comparative tests under suboptimal conditions (e.g., 50 mA/cm^2, 3 g/L NaCl, 4 h) yielded lower COD removal (92.3%), validating the necessity of balancing NaCl concentration and current density to avoid electrode passivation. Mechanistically, the optimal NaCl concentration (6.0 g/L) ensured sustained ClO^- production without salt-layer interference, while moderate current density (38 mA/cm^2) avoided energy-intensive mass transfer limitations (Anderson and Whitcomb, 2016). These findings confirm that RSM-derived parameters are not merely statistical abstractions but are experimentally robust and mechanistically grounded, providing actionable guidelines for efficient landfill leachate treatment.

4 Conclusions

This study systematically evaluates Ti/SnO_2-Sb_2O_3 and Ti/PbO_2 anodes for electrochemical oxidation (EO) of landfill leachate, revealing three critical findings:

1) Anode superiority: Ti/PbO_2 achieved 99.91% COD and 99.95% NH_4^+-N removal under optimized conditions (3 g/L NaCl, 65 mA/cm^2, 240 min), outperforming Ti/SnO_2-Sb_2O_3 (99.63% COD, 93.33% NH_4^+-N at 10 g/L NaCl, 65 mA/cm^2, 240 min).

2) Cathode optimization: Ni exhibited superior energy efficiency and efficacy over Pt and steel in EO systems.

3) Process drivers: Response surface analysis identified reaction time as the dominant control parameter ($P < 0.001$) for COD removal, with three-dimensional fluorescence confirming effective degradation of humic and fulvic acids.

The systematic comparative study offers more specific and practical criteria for the selection of anode and cathode materials, providing valuable insights for optimizing the treatment of landfill leachate.

Conflict of Interests Prof. Yongzhen Peng is an Advisory Board Member of *Frontiers of Environmental Science & Engineering*. The authors declare that they have no known competing financial interests or personal relationships that could have appeared to influence the work reported in this manuscript.

Acknowledgements This research was funded by the Project of the National Natural Science Foundation of China (Nos. 51678057 and 51208040); funded by the Project of Beijing Municipal Natural Science Foundation (China) (No. 8192010); and funded by the Fundamental Research Funds for Beijing University of Civil Engineering and Architecture (China) (X20074).

Electronic Supplementary Material Supplementary material is available in the online version of this article at https://doi.org/10.1007/s11783-025-1996-5 and is accessible for authorized users.

References

Abbasi A, Hosseini S, Somwangthanaroj A, Cheacharoen R, Olaru S, Kheawhom S (2020). Discharge profile of a zinc-air flow battery at various electrolyte flow rates and discharge currents. Scientific Data, 7(1): 196–204

Abdel-Shafy H I, Morsy R M, Hewehy M A, Razek T M, Hamid M M (2022). Treatment of industrial electroplating wastewater for metals removal via electrocoagulation continous flow reactors. Water Practice & Technology, 17(2): 555–566

Anderson M J, Whitcomb P J (2016). RSM Simplified: Optimizing Processes Using Response Surface Methods for Design of Experiments. 2nd ed. New York: Productivity Press

Bao H, Wu M, Meng X, Han H, Zhang C, Sun W (2023). Application of electrochemical oxidation technology in treating high-salinity organic ammonia-nitrogen wastewater. Journal of Environmental Chemical Engineering, 11(5): 110608

Chen D M C, Bodirsky B L, Krueger T, Mishra A, Popp A (2020a). The world's growing municipal solid waste: trends and impacts. Environmental Research Letters, 15(7): 074021

Chen J l (2008). Study and Application of Electrochemical Oxidation Technology for Ammonia Removal. Dissertation for the Doctoral Degree. Beijing: Tsinghua University (in Chinese)

Chen M, Pan S, Zhang C, Wang C, Zhang W, Chen Z, Zhao X, Zhao Y (2020b). Electrochemical oxidation of reverse osmosis concentrates using enhanced TiO_2-NTA/SnO_2-Sb anodes with/without PbO_2 layer. Chemical Engineering Journal, 399: 125756

Ciríaco L, Anjo C, Correia J, Pacheco M J, Lopes A (2009). Electrochemical degradation of Ibuprofen on Ti/Pt/PbO_2 and Si/BDD electrodes. Electrochimica Acta, 54(5): 1464–1472

Comninellis C (1994). Electrocatalysis in the electrochemical conversion/ combustion of organic pollutants for waste water treatment. Electrochimica Acta, 39(11/12): 1857–1862

Cossu R, Polcaro A M, Lavagnolo M C, Mascia M, Palmas S, Renoldi F (1998). Electrochemical treatment of landfill leachate: oxidation at Ti/PbO_2 and Ti/SnO_2 anodes. Environmental Science & Technology, 32(22): 3570–3573

De Brito R A, Filho H J I, Aguiar L G, De Alcântara M A K, Siqueira A F, Da Rós P C M (2019). Degradation kinetics of landfill leachate by continuous-flow catalytic ozonation. Industrial & Engineering Chemistry Research, 58(23):

9855–9863

Deng Y, Chen N, Feng C, Chen F, Wang H, Kuang P, Feng Z, Liu T, Gao Y, Hu W (2019). Treatment of organic wastewater containing nitrogen and chlorine by combinatorial electrochemical system: taking biologically treated landfill leachate treatment as an example. Chemical Engineering Journal, 364: 349–360

Deng Y, Englehardt J D (2007). Electrochemical oxidation for landfill leachate treatment. Waste Management, 27(3): 380–388

Duan X, Wang W, Wang Q, Sui X, Li N, Chang L (2020). Electrocatalytic degradation of perfluorooctane sulfonate (PFOS) on a 3D graphene-lead dioxide (3DG-PbO_2) composite anode: electrode characterization, degradation mechanism and toxicity. Chemosphere, 260: 127587

Fernandes A, Santos D, Pacheco M J, Ciríaco L, Lopes A (2014a). Nitrogen and organic load removal from sanitary landfill leachates by anodic oxidation at Ti/Pt/PbO_2, Ti/Pt/SnO_2-Sb_2O_4 and Si/BDD. Applied Catalysis B: Environmental, 148–149: 288–294

Fernandes A, Santos D, Pacheco M J, Ciríaco L, Lopes A (2016). Electrochemical oxidation of humic acid and sanitary landfill leachate: Influence of anode material, chloride concentration and current density. Science of the Total Environment, 541: 282–291

Fernandes A, Spranger P, Fonseca A D, Pacheco M J, Ciríaco L, Lopes A (2014b). Effect of electrochemical treatments on the biodegradability of sanitary landfill leachates. Applied Catalysis B: Environmental, 144: 514–520

Fu R, Zhang P S, Jiang Y X, Sun L, Sun X H (2023). Wastewater treatment by anodic oxidation in electrochemical advanced oxidation process: advance in mechanism, direct and indirect oxidation detection methods. Chemosphere, 311: 136993

He X S, Xi B D, Li X, Pan H W, An D, Bai S G, Li D, Cui D Y (2013). Fluorescence excitation–emission matrix spectra coupled with parallel factor and regional integration analysis to characterize organic matter humification. Chemosphere, 93(9): 2208–2215

He X S, Xi B D, Wei Z M, Jiang Y H, Yang Y, An D, Cao J L, Liu H L (2011). Fluorescence excitation–emission matrix spectroscopy with regional integration analysis for characterizing composition and transformation of dissolved organic matter in landfill leachates. Journal of Hazardous Materials, 190(1−3): 293–299

He X S, Yu J, Xi B D, Jiang Y H, Zhang J B, Li D, Pan H W, Liu H L (2012). The remove characteristics of dissolved organic matter in landfill leachate during the treatment process. Spectroscopy and Spectral Analysis, 32(9): 2528–2533

He Y, Lin H, Guo Z, Zhang W, Li H, Huang W (2019). Recent developments and advances in boron-doped diamond electrodes for electrochemical oxidation of organic pollutants. Separation and Purification Technology, 212: 802–821

Iovino P, Fenti A, Galoppo S, Najafinejad M S, Chianese S, Musmarra D (2023). Electrochemical removal of nitrogen compounds from a simulated saline wastewater. Molecules, 28(3): 1306

Kapałka A, Fóti G, Comninellis C (2010). Electrochemistry for the Environment. Berlin: Springer

Kan X, Yu X, Zhao W, Lyu S, Sun S, Yu G, Sui Q (2023). Screening of indicator pharmaceuticals and personal care products in landfill leachates: a case study in Shanghai, China. Frontiers of Environmental Science & Engineering, 17(9): 116

Komatsu K, Onodera T, Tsuchiya K, Kohzu A, Syutsubo K (2025). Identification of wastewater-specific peak on eem and their application for detecting the effluent in the discharged area. Water Research, 275: 123213

Lee K M, Lee H J, Seo J, Lee T, Yoon J, Kim C, Lee C (2022). Electrochemical oxidation processes for the treatment of organic pollutants in water: performance evaluation using different figures of merit. ACS ES&T Engineering, 2(10): 1797–1824

Li X, Ren Y, Chen X, Li Y, Chertow Marian R (2023). Exploring the development of municipal solid waste disposal facilities in Chinese cities: patterns and drivers. Frontiers of Environmental Science & Engineering, 17(11): 139

Liu Z J, Luo X, Shao S L, Xia X (2023). Electrocatalytic reduction of nitrate using Pd-Cu modified carbon nanotube membranes. Frontiers of Environmental Science & Engineering, 17(4): 40

Lindamulla L, Nanayakkara N, Othman M, Jinadasa S, Herath G, Jegatheesan V (2022). Municipal solid waste landfill leachate characteristics and their treatment options in tropical countries. Current Pollution Reports, 8(3): 273–287

Luu T L (2020). Post treatment of ICEAS-biologically landfill leachate using electrochemical oxidation with Ti/BDD and Ti/RuO_2 anodes. Environmental Technology & Innovation, 20: 101099

Mandal P, Gupta A K, Dubey B K (2020). Role of inorganic anions on the performance of landfill leachate treatment by electrochemical oxidation using graphite/PbO_2 electrode. Journal of Water Process Engineering, 33: 101119

Miao L, Zhang Q, Wang S, Li B, Wang Z, Zhang S, Zhang M, Peng Y (2018). Characterization of EPS compositions and microbial community in an anammox SBBR system treating landfill leachate. Bioresource Technology, 249: 108–116

Panizza M, Martinez-Huitle C A (2013). Role of electrode materials for the anodic oxidation of a real landfill leachate-comparison between Ti–Ru–Sn ternary oxide, PbO_2 and boron-doped diamond anode. Chemosphere, 90(4): 1455–1460

Qiang Z, Adams C D (2004). Determination of monochloramine formation rate constants with stopped-flow spectrophotometry. Environmental Science & Technology, 38(5): 1435–1444

Rao X, Shao X, Xu J, Yi J, Qiao J, Li Q, Wang H, Chien M, Inoue C, Liu Y, et al. (2019). Efficient nitrate removal from water using selected cathodes and Ti/PbO_2 anode: experimental study and mechanism verification. Separation and Purification Technology, 216: 158–165

Rigotto L, Aquino S F, Rigotto J, Santos G, Silva L M, Santiago A F (2023). Dynamics of dissolved organic matter (DOM) in waste stabilization ponds: insights into co-treatment of sanitary sewage

and landfill leachate. Journal of Water Process Engineering, 55: 104236

Särkkä H, Bhatnagar A, Sillanpää M (2015). Recent developments of electro-oxidation in water treatment: a review. Journal of Electroanalytical Chemistry, 754: 46–56

Sharma K, Sudhaik A, Kumar R, Nguyen V H, Van Le Q, Ahamad T, Thakur S, Kaya S, Nguyen L H, Raizada P, et al. (2024). Advanced photo-Fenton assisted degradation of tetracycline antibiotics using α-Fe_2O_3/CdS/SiO_2 based S-scheme photocatalyst. Journal of Water Process Engineering, 59: 105011

Shih Y J, Hsu C H (2021). Kinetics and highly selective N_2 conversion of direct electrochemical ammonia oxidation in an undivided cell using NiCo oxide nanoparticle as the anode and metallic Cu/Ni foam as the cathode. Chemical Engineering Journal, 409: 128024

Sun J, Liu L, Yang F (2021). Electro-enhanced chlorine-mediated ammonium nitrogen removal triggered by an optimized catalytic anode for sustainable saline wastewater treatment. Science of the Total Environment, 776: 146035

Sun H (2008). Research on Ultrasonic and Electrical Oxidation Degradation of Azo Dyes Wastewater. Thesis for the Master's Degree. Nanjing: Nanjing University of Aeronautics and Astronautics (in Chinese)

Tien T T, Luu T L (2020). Electrooxidation of tannery wastewater with continuous flow system: role of electrode materials. Environmental Engineering Research, 25(3): 324–334

Van Ede M C, Fichtner A, Angst U (2024). Nondestructive detection and quantification of localized corrosion rates by electrochemical tomography. NDT & E International, 142: 103005

Wang B H, Zhao P Y, Zhang X N, Zhang Y, Liu Y M (2024). Three-dimensional electro-Fenton system with iron-carbon packing as a particle electrode for nitrobenzene wastewater treatment. Frontiers of Environmental Science & Engineering, 18(11): 138

Wang K, Qin X, Cao P (2023). High-efficiency refractory organic pollutants removal boosted by combining heterogeneous electro-fenton with electrochemical anodic oxidation over a broad ph range. Process Safety and Environmental Protection, 177: 635–642

Wu L, Shen M, Li J, Huang S, Li Z, Yan Z, Peng Y (2019). Cooperation between partial-nitrification, complete ammonia oxidation (comammox), and anaerobic ammonia oxidation (anammox) in sludge digestion liquid for nitrogen removal. Environmental Pollution, 254: 112965

Xi B D, He X S, Wei Z M, Jiang Y H, Li M X, Li D, Li Y, Dang Q L (2012). Effect of inoculation methods on the composting efficiency of municipal solid wastes. Chemosphere, 88(6): 744–750

Zhao G, Zhang Y, Lei Y, Lv B, Gao J, Zhang Y, Li D (2010). Fabrication and electrochemical treatment application of a novel lead dioxide anode with superhydrophobic surfaces, high oxygen evolution potential, and oxidation capability. Environmental Science & Technology, 44(5): 1754–1759

Zhao R, Liu J, Feng J, Li X, Li B (2021). Microbial community composition and metabolic functions in landfill leachate from different landfills of China. Science of the Total Environment, 767: 144861

Zheng R, Zhang K, Kong L, Liu S (2024). Research progress and prospect of low-carbon biological technology for nitrate removal in wastewater treatment. Frontiers of Environmental Science & Engineering, 18(7): 80

Zhou W, Liu W, Qin M, Chen Z, Xu J, Cao J, Li J (2020). Fundamental properties of TEMPO-based catholytes for aqueous redox flow batteries: effects of substituent groups and electrolytes on electrochemical properties, solubilities and battery performance. RSC Advances, 10(37): 21839–21844

Zhu X, Tong M, Shi S, Zhao H, Ni J (2008). Essential explanation of the strong mineralization performance of boron-doped diamond electrodes. Environmental Science & Technology, 42(13): 4914–4920